RESEARCH ARTICLE

JCN RESEARCH IN SYSTEMS NEUROSCIENCE THE JOURNAL OF COMPARATIVE NEUROLOGY   WILEY

Modeling human-specific interlaminar astrocytes in the mouse cerebral cortex

Ragunathan Padmashri[1]† | Baiyan Ren[2]† | Braden Oldham[1] | Yoosun Jung[1] | Ryan Gough[1] | Anna Dunaevsky[1] [ID]

[1]Department of Neurological Sciences, University of Nebraska Medical Center, Omaha, Nebraska

[2]Department of Biochemistry and Molecular Biology, University of Nebraska Medical Center, Omaha, Nebraska

Correspondence
Anna Dunaevsky, Department of Neurological Sciences, University of Nebraska Medical Center, Omaha, NE.
Email: adunaevsky@unmc.edu

Abstract

Astrocytes, a highly heterogeneous population of glial cells, serve as essential regulators of brain development and homeostasis. The heterogeneity of astrocyte populations underlies the diversity in their functions. In addition to the typical mammalian astrocyte architecture, the cerebral cortex of humans exhibits a radial distribution of interlaminar astrocytes in the supragranular layers. These primate-specific interlaminar astrocytes are located in the superficial layer and project long processes traversing multiple layers of the cerebral cortex. However, due to the lack of accessible experimental models, their functional properties and their role in regulating neuronal circuits remain unclear. Here we modeled human interlaminar astrocytes in humanized glial chimeric mice by engrafting astrocytes differentiated from human-induced pluripotent stem cells into the mouse cortex. This model provides a novel platform for understanding neuron-glial interaction and its alterations in neurological diseases.

KEYWORDS
astrocytes, cortex, interlaminar, iPSC, primate

1 | INTRODUCTION

Astrocytes, a subtype of glial cells in the central nervous system, play an essential role in maintaining homeostasis of the Central Nervous System (CNS) (Verkhratsky & Nedergaard, 2018). Astrocytes are tightly integrated into the neural circuits and regulate various aspects of CNS function, including modulation of neuronal development (Baldwin & Eroglu, 2017; Vainchtein et al., 2018; Van Horn & Ruthazer, 2018) and synaptic transmission (Krencik, van Asperen, & Ullian, 2017), regulation of ionic homeostasis (Olsen et al., 2015), recycling of neurotransmitters (Araque, Li, Doyle, & Haydon, 2000), regulation of metabolism and maintenance of the blood–brain barrier (Sofroniew & Vinters, 2010). Cumulative evidence revealed that different morphologies and transcriptomes of astrocyte subtypes enriched in different brain regions contribute to the heterogeneity of astrocytic functions (Khakh & Deneen, 2019; Khakh & Sofroniew, 2015; Oberheim, Goldman, & Nedergaard, 2012). However, most results were derived from rodent astrocytes, which have interspecies differences with human astrocytes (Hodge et al., 2019; Oberheim et al., 2009; Zhang et al., 2016) and the structural and functional properties of human astrocytes remain mainly unknown.

Compared with rodent counterparts, human astrocytes have specific genomic profiles, more extensive territories, more complex morphologies, faster intracellular Ca^{2+} signal propagation, as well as primate-specific morphologies (Oberheim et al., 2009; Oberheim, Wang, Goldman, & Nedergaard, 2006; Zhang et al., 2016). Multiple subtypes of astrocytes are distributed in different brain regions, including protoplasmic

astrocytes in the gray matter, fibrous astrocytes in the white matter, velate astrocytes, perivascular astrocytes, Muller astrocytes, Bergman glia, and others (Verkhratsky & Nedergaard, 2018). While the above-mentioned astrocytes are found in all mammals, interlaminar and varicose projection astrocytes are higher-order primate and human-specific, respectively (Colombo, Gayol, Yanez, & Marco, 1997; Colombo, Lipina, Yanez, & Puissant, 1997; Falcone et al., 2019; Oberheim et al., 2009; Verkhratsky & Nedergaard, 2018). In the human cortex, typical inter-laminar astrocytes reside in layer I and project long processes that traverse multiple laminae, terminating in layer III/IV (Colombo & Reisin, 2004; Falcone et al., 2019). Although a subtype of rudimentary interlaminar astrocytes with soma located in the superficial layer was also described recently in the rodent cortex, their processes are short and do not extend beyond layer 1 (Falcone et al., 2019). Due to the lack of a tractable experimental model, the role of primate-specific typical interlaminar astrocytes in the development, maintenance, and function of cortical neural circuits remains obscure.

Astrocytes ensheath neuronal synapses and are also in direct contact with blood vessels, consequently forming an integral component of the nervous system architecture. The radial distribution and the length of the interlaminar processes suggest that they participate in modulating neuronal columnar organization, and might underlie long-distance astrocytic regulation in the human cerebral cortex. The absence of typical interlaminar astrocytes in rodents has hampered the progress in testing these functional hypotheses. The differentiation of astrocytes from human-induced pluripotent stem cells (hiPSCs) promoted research of the role of human astrocytes in brain development and neurological diseases (Canals et al., 2018; Chen et al., 2014; Jones, Atkinson-Dell, Verkhratsky, & Mohamet, 2017; Oksanen et al., 2017; Russo et al., 2017; Windrem et al., 2017). However, most studies were performed on pan-astrocytes growing in a dish, rather than in the physiological brain environment, making it challenging to model astrocyte subtypes and understand their functions. Although interlaminar processes have been reported following engraftment of human glial progenitors into the mouse brain, the typical "palisade-like" organization was not observed (Han et al., 2013). To study the role of interlaminar astrocytes in the developing and intact brain, a model with a better anatomical fidelity of interlaminar astrocytes is needed.

Here, we generated a model to develop interlaminar astrocytes in the mouse cerebral cortex by combining hiPSCs differentiation and human-mouse chimera approach. We report that the distribution pattern and morphology of interlaminar astrocytes in the chimeric mouse brain resemble that of the human brain, engendering it possible to study the anatomical and functional properties of human-exclusive interlaminar astrocytes in easily accessible mouse cortex.

2 | METHODS

2.1 | Mice

Mice were cared in accordance with NIH guidelines for laboratory animal welfare. All protocols were approved by the University of Nebraska Medical Center (UNMC) Institutional Animal Care and Use Committee. Rag1 immunodeficient mice (B6.129S7-$Rag1^{tm1Mom}$/J, Jackson Laboratory, IMSR Cat# JAX: 002216, RRID: IMSR_JAX: 002216) were bred at the UNMC facility with a 12-hr light/dark cycle with food and water available ad libitum.

2.2 | Stem cell differentiation

FX11-9u hiPSC line (RRID: CVCL_EJ77) was obtained from WiCell. The xeno-free, chemically defined astrocyte differentiation method previously described (Chen et al., 2014) was modified in our study. Briefly, hiPSCs were cultured in the feeder-free maintenance medium mTeSR™ Plus (STEMCELL Technologies, 05825) on Matrigel (Corning, 354277)-coated dishes. The colonies of hiPSCs were split manually after treating with Dispase (1 U/ml, STEMCELL Technologies, 07923) to generate the embryoid bodies. Embryoid bodies were grown in suspension culture in DME/F-12 (Hyclone, SH3002301), with 1× N2 supplement (Invitrogen, 17502048) and Noggin (40 ng/ml, PeproTech, #120-10C) for 3–5 days. Embryoid bodies were then plated on growth factor reduced Matrigel (Corning, 354230)-coated dishes in DME/F12, 1× N2 supplement, and laminin (1 μg/ml, Invitrogen, 2317-015). NPCs formed neural rosettes after growing for another 1 week. Manually isolated NPCs were expanded as neurospheres in suspension culture for 1 week in the presence of NPC medium, composed of DME/F12 and Neurobasal medium (Invitrogen, 21103-049) in the ratio of 1:1, supplemented with 1× N2, 1× B27 (without vitamin A, Invitrogen, 12587-010), and FGF-basic (20 ng/ml, PeproTech, 100-18B). To differentiate astrocytes, neurospheres were dissociated into single cells and were cultured on growth factor reduced Matrigel-coated dishes in astrocyte differentiation medium, consisting of DME/F12, 1× N2 supplement, 1× B27-RA supplement, BMP4 (10 ng/ml, Peprotech, 120-05ET), and FGF-basic (20 ng/ml). For hiPSCs, embryoid bodies, and neurospheres, culture medium was changed every day. For neural rosettes and astrocyte culture, the medium was changed every other day.

2.3 | Viral transduction

NPCs were plated in growth factor reduced Matrigel-coated 24-well plates at a density of 1×10^6 cells/well. After 24 hr, the NPC medium in the plate was changed to an astrocyte differentiation medium. After 24 hr the medium in each well was replaced to 1 ml fresh astrocyte differentiation medium containing 1.25 μl of CMV-RFP lentivirus (1×10^8 TU/ml, Cellomics Technology) and 8 μg/ml polybrene (Sigma-Aldrich, TR-1003-G). Following a 6-hr incubation, the medium was replaced with fresh astrocyte differentiation medium. The medium was changed daily for 3 days to remove dead cells. Transduced cells were selected on days 4–8 post-transduction by gradually increasing the concentration of Puromycin (1-4 μg/ml). Sixteen to twenty days after transduction, a mixture of RFP-expressing and non-RFP-expressing astrocytes were harvested for engraftment.

2.4 | Immunocytochemistry

Nineteen days after transduction, hiPSC-astrocytes were plated on growth factor reduced Matrigel-coated 1 mm coverslips placed in 24-well plates at a density of 5×10^5 cells/coverslip. After 24 hr, the cells were fixed with 4% paraformaldehyde in phosphate buffer (0.1 M), permeabilized with 0.1% Triton-X-100 (BP151-100), treated with blocking buffer (phosphate-buffered saline [1xPBS] containing 5% normal goat serum and 0.1% Triton-X-100) for 1 hr at room temperature, and incubated with primary antibodies overnight at 4°C. Secondary antibodies were applied for 1 hr at room temperature and coverslips were mounted in Fluoromount-G™ with DAPI (00-4959-52).

The primary antibodies used were chicken anti-RFP (Rockland Cat# 600-901-379, RRID: AB_10704808), 1:500; rabbit anti-ALDH1L1 (abcam, ab190298, RRID: AB_2857848), 1:500; mouse anti-GFAP (UC Davis/NIH NeuroMab Facility Cat# 75-240, RRID: AB_10672299), 1:300; rabbit anti-S100 (Abcam Cat# ab868, RRID: AB_306716), 1:100. All the secondary antibodies were goat anti-chicken Alexa Fluor 594 (Thermo Fisher Scientific Cat# A-11042, RRID: AB_2534099), goat anti-mouse Alexa Fluor 594 (Thermo Fisher Scientific Cat# A-11005, RRID: AB_2534073), goat anti-rabbit Alexa Fluor 488 (Thermo Fisher Scientific Cat# A-11008, RRID:AB_143165) and were used at dilution of 1:1000.

2.5 | Engraftment of human iPSC derived astrocytes

Rag1$^{-/-}$ neonatal mice (total of 8, both males and females) were transplanted on postnatal day 1 with hiPSC-derived astrocytes expressing RFP. The pups were cryoanesthetized for 4 min and transferred to a neonatal stage (Stoelting) that was cooled to 4°C during the stereotaxic injections. For cortical labeling, the pups were injected directly through the skin into two sites: AP −1.0 and − 2.0, ML ± 1.0 mm, ventral 0.2–0.8 mm, 10,000 cells/μl per site using a Hamilton syringe.

2.6 | Tissue preparation and immunohistochemistry

Mice were deeply anesthetized with TribromoEthanol (Avertin, 400 mg/kg i.p.) and transcardially perfused with 4% paraformaldehyde in phosphate buffer (0.1 M) at 3, 6, and 9 months post engraftment. The brain was dissected, postfixed overnight, and 100 μm sagittal sections were cut on a vibratome in PBS. Sections from the chimeric mice were processed for immunostaining as previously described (Coiro et al., 2015) with mouse anti-human GFAP (BioLegend Cat# 837202, RRID:AB_2565372), 1:1000; chicken anti-RFP (Rockland Cat# 600–901-379, RRID: AB_10704808), 1:500; rabbit anti-GFAP (Agilent Cat# Z0334, RRID:AB_10013382), 1:300; mouse anti-human

nuclei (Millipore Cat# MAB4383, RRID:AB_827439), 1:250; rabbit anti-AQP4 (Alomone Labs Cat# AQP-004, RRID:AB_2039734), 1:200; rabbit anti-Kir4.1 (Alomone Labs Cat# APC-035, RRID:AB_2040120), 1:200; mouse anti-hCD44 (Abcam Cat# ab6124, RRID:AB_305297), 1:200; rabbit anti-S100B (Abcam Cat# ab868, RRID:AB_306716), 1:100; guinea pig anti-vGluT1 (Millipore Cat# AB5905, RRID: AB_2301751), 1:300. Secondary antibodies (Invitrogen) were used at the following dilutions: goat anti-mouse Alexa Fluor 488 (Thermo Fisher Scientific Cat# A-11001, RRID:AB_2534069; 1:200 and 1:1000), goat anti-chicken Alexa Fluor 594 (Thermo Fisher Scientific Cat# A-11042, RRID:AB_2534099; 1:1000), goat anti-rabbit Alexa Fluor 488 (Thermo Fisher Scientific Cat# A-11008, RRID:AB_143165; 1:400, 1:500 and 1:1000), goat anti-mouse Alexa Fluor 647 (Thermo Fisher Scientific Cat# A-21235, RRID:AB_2535804; 1:500) and goat anti-guinea pig Alexa Fluor 647 (Thermo Fisher Scientific Cat# A-21450, RRID:AB_2735091, 1:300).

2.7 | Human tissue

Human postmortem brain tissue was acquired from Harvard Brain Tissue Resource Center and the NIH NeuroBioBank. The formalin-fixed paraffin-embedded human postmortem brain tissues from three donors (S11723-18 years old, S08652-17 years old, S17215-16 years old) from Brodmann areas 3, 1, 2 was sectioned at 10 μm, and immunostained with mouse anti-human GFAP.

2.8 | Confocal imaging and image analysis

Confocal imaging of cells on coverslips was performed on a Zeiss LSM 700 confocal microscope with 20x (0.5NA) objectives. Images were collected at 1024 × 1024 pixels (with a pixel size of 0.31 μm) with 405, 488, 555 nm lasers.

Confocal imaging of tissue sections was performed on a Nikon A1R upright microscope and images were acquired using a 20x (0.75 NA) and 40x oil (1.3 NA) objectives. Images were collected at 512 × 512 pixels (with a pixel size of 1.24 μm and 0.62 μm for 20x and 40x, respectively) and a step size of 1 μm with 488, 561 and 640 nm lasers. The step size for VGlut1 imaging was 0.2 μm.

Image analysis was performed using ImageJ. To estimate the distance traversed by the interlaminar processes across the cortical layers, the plot profile function was used. The analysis was performed on 6–9 sections per mouse with 2–3 mice at 3, 6, and 9-month time points and 1–2 positions per human postmortem brain tissue from three donors. In each section multiple 5-pixel broad straight lines, 150–200 μm apart, were drawn from the pial surface to the deeper layer. For each line, the plot profile function was used to estimate the pixel intensity values along the line. The location of the last peak of RFP or GFAP fluorescence was used as a measure of the extent to which processes traversed across the cortex and averaged per section.

2.9 | Statistical analysis

Data are reported as mean ± *SEM*. Normal distribution was tested using the Kolmogorov–Smirnov test. The analysis was done using one-way ANOVA with Sidak's multiple comparison test. Data were analyzed using GraphPad Prism.

3 | RESULTS

### 3.1 | Generation of hiPSCs-astrocyte chimeric mice

We differentiated human-induced pluripotent stem cells (hiPSCs) to neural progenitor cells (NPCs), and astrocytes subsequently, via a xeno-free, chemically defined method (Figure 1a) (Chen et al., 2014). To visualize the hiPSC-astrocytes in the chimeric mouse brain, we generated RFP-expressing astrocytes by transducing NPCs with lentivirus expressing RFP in the presence of the astrocyte differentiation medium (Figure 1a). Before engraftment, RFP-expressing hiPSC-astrocytes showed robust expression of canonical markers, including aldehyde dehydrogenase 1 family member L1 (ALDH1L1), glial fibrillary acidic protein (GFAP), and S100 calcium-binding protein B (S100B) (Figure 1b). The RFP-expressing hiPSC-derived immature astrocytes were engrafted into the cortex of postnatal day 1 (P1) $rag1^{-/-}$ immunodeficient mouse brains (Figure 2a). Two-site injection resulted in the widespread distribution of RFP-expressing hiPSC-astrocytes in the frontal cortex (Figure 2b,c). In the un-injected hemisphere of the same chimeric mice, GFAP immunostaining revealed only the recently described mouse rudimentary interlaminar astrocytes (Falcone et al., 2019), with very short processes that do not exit layer I, as well as the typical protoplasmic astrocytes in other cortical layers (Figure 3d). While at what are likely to be sites of engraftment of hiPSC-astrocytes, thick bands of cell bodies are found in the superficial cortex, further away, cells are mainly confined to layer 1 (Figure 2c and Figure 3). In addition, while cells with interlaminar processes are found in the superficial layers, protoplasmic astrocytes can be observed in the deeper layers at putative sites of injection (Figure 2c,d).

3.2 | Timeline of interlaminar astrocyte development in the chimeric mouse

To follow the development of interlaminar astrocytes in the chimeric mouse brain, we focused our study on three-, six- and nine-month post-engraftment. We observed that cell bodies of the interlaminar astrocytes resided both at the pial surface and within layer 1 (Figure 3a–c), similar to the pial and subpial interlaminar astrocytes described in the primate cortex (Falcone et al., 2019). Three months after engraftment, hiPSC-astrocytes showed short processes confined to layer I (Figure 3a). Six months after engraftment, a few long processes traversing into deep layers were observed (Figure 3b). After 9-month development in the chimeric mouse cortex, hiPSC-astrocytes showed interlaminar processes with "palisade-like" distribution that traversed multiple layers of the mouse cortex (Figure 3c). These were similar to the GFAP-immunoreactive interlaminar astrocytes with long processes that were previously described (Oberheim et al., 2009) and which we also observed in a normal 16-year-old human cortical section (Brodmann areas 3, 1, 2) (Figure 3e). These results indicated that the distribution pattern of hiPSC-astrocytes in the chimeric mouse cortex mimics that of the human cortex.

To further characterize the interlaminar astrocytes in the chimeric mouse cortex, we measured the average distance traversed by the
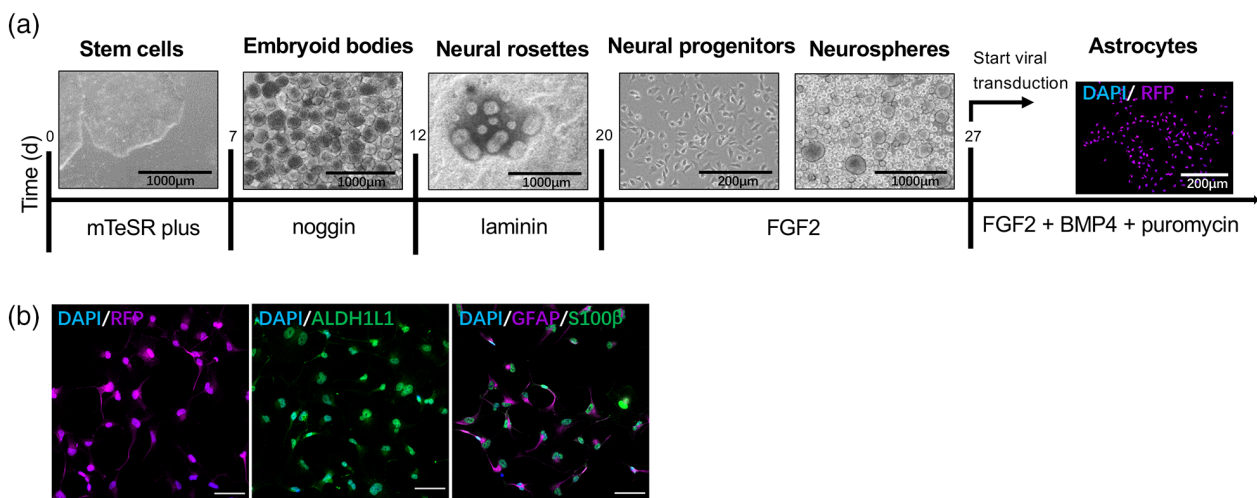
FIGURE 1 Generation of hiPSC-astrocytes. (a) Schematic of hiPSC differentiation and RFP viral transduction. (b) Expression of RFP (left), ALDH1L1 (middle), GFAP and S100B (right) in astrocytes before engraftment (here shown for D20–D22). Scale = 200 μm [Color figure can be viewed at wileyonlinelibrary.com]
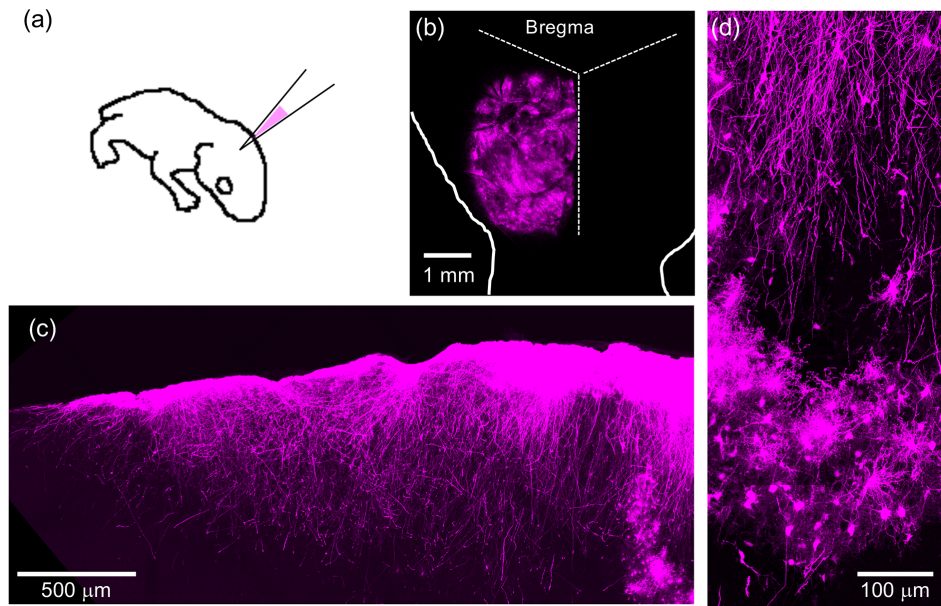
FIGURE 2 Chimeric mice engrafted with hiPSC-astrocytes develop interlaminar processes. (a) Schematic of engraftment of hiPSC-astrocytes. (b) Whole mount view of a brain from a 9-month-old mouse engrafted with RFP expressing hiPSC-astrocytes. The dashed lines mark the skull sutures and the solid line outlines the brain. (c) Sagittal section from a 9-month engrafted mouse with RFP-expressing hiPSC-astrocytes. Interlaminar astrocytes are seen throughout the anterior–posterior (right–left) area. Protoplasmic astrocytes can be seen in deeper cortical layers in the anterior portion of the section closer to the injection site. (d) Higher magnification image of protoplasmic astrocytes below the interlaminar processes [Color figure can be viewed at wileyonlinelibrary.com]
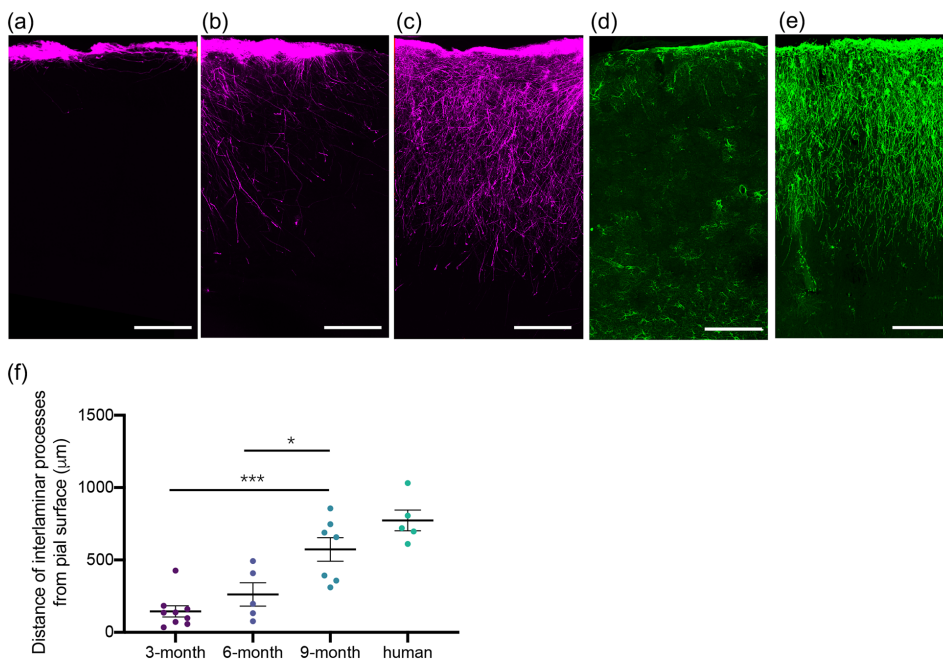
FIGURE 3 Developmental time-course of interlaminar astrocyte processes in the chimeric mouse cortex. (a–c) hiPSC-astrocytes expressing RFP in the cortex of 3-, 6-, and 9-month old chimeric mice. (d) Mouse rudimentary interlaminar astrocytes immunostained with GFAP in the un-injected hemisphere of a chimeric mouse. (e) Interlaminar astrocytes in the human cortex immunostained with hGFAP. (f) Quantification of the distance traversed by interlaminar processes in the mouse cortex at different ages and in the adult human cortex (N = 5–9 sections from 2 to 3 chimeric mice per age group, and N = 5 fields from three sections of human postmortem tissue). Scale = 200 μm [Color figure can be viewed at wileyonlinelibrary.com]

interlaminar processes from the pial surface and compared with that of human cortex. Because of the large number of processes in the "palisade-like" distribution, we were not able to reliably follow the processes of individual cells, instead we measured the distance of the "interlaminar palisade" from the pial surface. In the chimeric mouse

cortex, the average distance that interlaminar processes traversed increased with age, reaching 145.00 ± 38.81 μm, 261.7 ± 80.64 μm, and 572.7 ± 81.49 μm at the 3-, 6-, and 9-month time points following engraftment, respectively. Although in the human cortex from 16 to 18 years subjects the interlaminar astrocyte processes were longer,
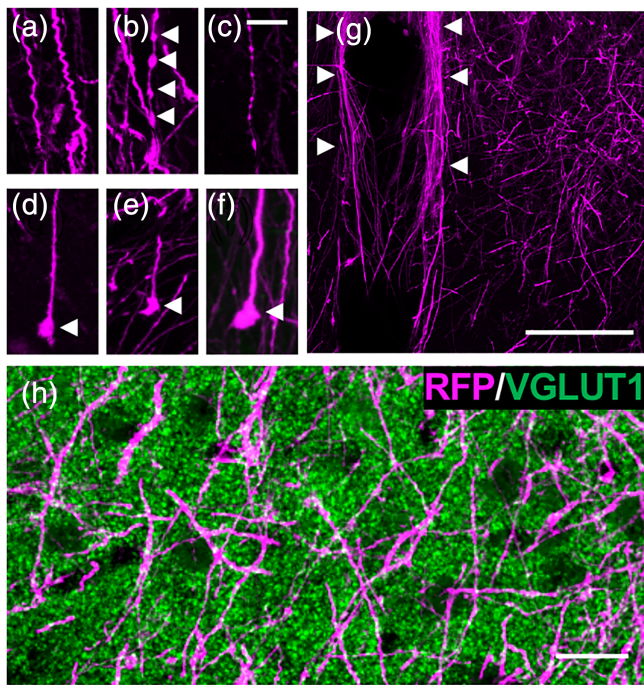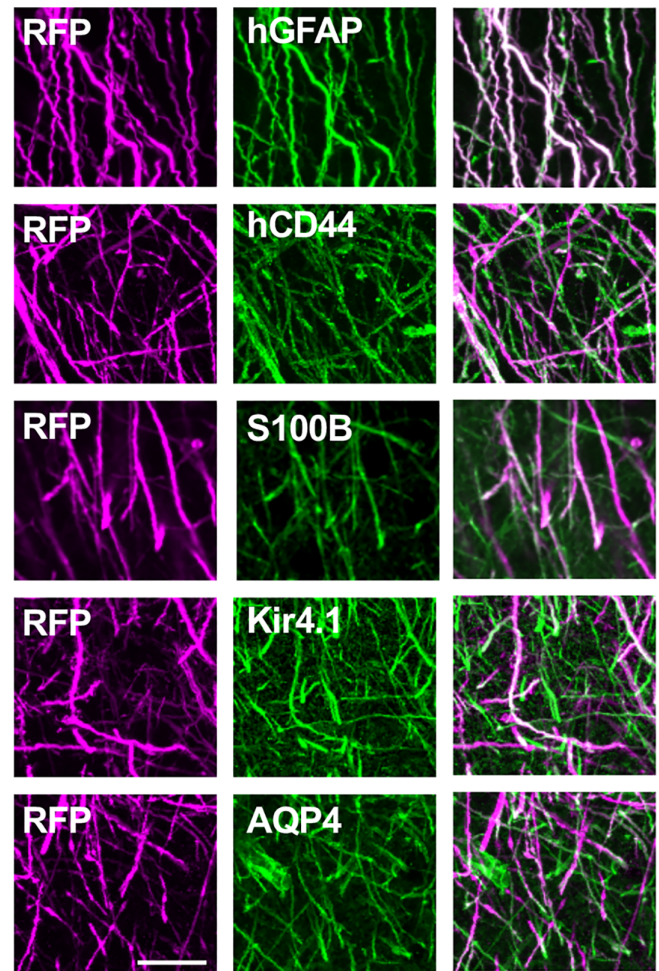
FIGURE 4 Interlaminar astrocytes in the mouse cortex exhibit typical features. (a) Tortuous appearance of interlaminar processes. (b, c) Interlaminar processes decorated by varicosities (arrow heads). (d–f) Terminal bulbs (arrowheads) on interlaminar processes. (g) Interlaminar processes line blood vessels (arrowhead). (h) Interlaminar processes interact with VGLUT1 labeled presynaptic terminals. Scale = 10 μm for (a–f) and (h); 100 μm for (g) [Color figure can be viewed at wileyonlinelibrary.com]

FIGURE 5 Interlaminar astrocytes in the mouse cortex express canonical astrocytic markers. Sections from 9-month-old mouse engrafted with RFP expressing hiPSC-astrocytes and immunostained with the antibodies against hGFAP, hCD44, S100B, Kir4.1, and AQP4. Scale = 10 μm [Color figure can be viewed at wileyonlinelibrary.com]

reaching an average distance of 773.4 ± 71.65 μm (Figure 3f), at 9 months following engraftment, some interlaminar processes reached distances of over 1 mm, identical to what was observed in adult human cortex (Colombo, Gayol, et al., 1997).

3.3 | Morphological features of hiPSC-derived interlaminar astrocytes

We observed that the interlaminar processes of hiPSC-astrocytes in the chimeric mouse cortex shared typical features with interlaminar astrocytes in the primate cortex. Processes of primate interlaminar astrocytes have been described as highly tortuous. The same feature was observed in a subset of hiPSC-astrocytes (Figure 4a). Additionally, we observed the existence of varicosities along with these processes, which is a feature that was observed in varicose projection astrocytes (Figure 4b,c) (Oberheim et al., 2009). Similar to the primate cortex, interlaminar hiPSC-astrocytes in the chimeric mouse cortex displayed bulbous endings in layer V after 6 months after engraftment (Figure 4d–f). Interlaminar astrocyte processes also line blood vessels, which can be observed both from the whole brain surface view (Figure 2b) and in the brain sections (Figure 4g), mimicking the

astrocyte architecture in the primate cortex (Colombo, Lipina, et al., 1997). Finally, interlaminar astrocyte processes appear to integrate into the brain parenchyma, interacting with presynaptic terminals labeled with vesicular marker VGLUT1 (Figure 4h).

3.4 | Interlaminar astrocytes express canonical astrocytic markers

Finally, to characterize hiPSC-derived interlaminar astrocytes on a molecular level and to verify their astrocytic nature, we performed colocalization studies with astroglia markers. Processes of hiPSC-derived interlaminar astrocytes (RFP positive and negative) expressed GFAP, CD44, S-100B, inwardly rectifying potassium channel (Kir4.1), and aquaporin-4 (AQP4) (Figure 5). This expression pattern agrees with the astrocyte phenotype of hiPSC-derived interlaminar astrocytes.

4 | DISCUSSION

The species-specific features of primate interlaminar astrocytes suggest an essential role in the advanced cognitive ability of primates, compared with other non-primate mammals. However, due to the lack of experimental models, our current knowledge of the primate interlaminar astrocytes development, functional properties, and roles in neuronal circuit function remains largely unknown. Here, we report the generation of a hiPSC-based chimeric mouse model, which results in the development of interlaminar astrocytes in the cortex that closely mimics the interlaminar astrocytes observed in the cerebral cortex of humans and other primates.

Astrocytes are generated from the same population of multipotent neural progenitor cells (NPCs) as neurons (Taupin & Gage, 2002), with astrogenesis following neurogenesis (Bayer & Altman, 1991; Forscher & Smith, 1988; Hirabayashi & Gotoh, 2005; Miller & Gauthier, 2007). Intermediate glial progenitor cells, develop into immature proliferative astrocytes; which migrate through cortical layers while continuing to proliferate (Verkhratsky & Nedergaard, 2018). The RFP-expressing hiPSC-astrocytes we engrafted are immature proliferative astrocytes. Based on our results of widespread localization of interlaminar astrocytes following two injection sites, we surmise that the cells that were engrafted into the most superficial layers continued to proliferate and migrate either along the pial surface or within the superficial layer 1 and gave rise to the interlaminar astrocytes. Cells that were engrafted in deeper cortical layers developed into protoplasmic astrocytes and were more limited in their migration. Thus, local cues likely regulate the identity and morphological attributes of the engrafted hiPSC-astrocytes.

In the human cerebral cortex, GFAP-immunoreactive interlaminar processes were described to emerge as early as postnatal day 10 (Colombo, Gayol, et al., 1997), and begin to develop into adult-like palisade configuration by postnatal day 60 (Colombo, Reisin, Jones, & Bentham, 2005). In the chimeric mouse model, human astrocytes are enriched in the superficial layer at 3-month post-engraftment, yet we did not observe the development of interlaminar processes until 6-month post-engraftment. The delayed development of interlaminar astrocytes in the chimeric mouse brain suggests that human-specific extrinsic factors could regulate the timing of the transition from "pre-palisade" to palisade morphology (Colombo et al., 2005).

Although the processes of interlaminar hiPSC-astrocytes extended to a distance of ∼600 μm from the pial surface at 9 months following engraftment, we also observed processes that traversed distances over 1,000 μm. This is similar to what is observed in humans, where over 1 mm processes are observed (Colombo, Lipina, et al., 1997), suggesting that the factors regulating the length of the human interlaminar astrocyte processes are conserved in the mouse brain. Interestingly, it was reported that the presence and length of interlaminar processes are affected by thalamic afferents (Reisin & Colombo, 2004). Similar to primates (Colombo, Lipina, et al., 1997), interlaminar astrocytes in the chimeric mouse cortex projected tortuous processes in a radial pattern with some ending with a bulbous structure, suggesting that these two features are either intrinsic

properties or, if extrinsic, are not altered by the mouse cerebral cortex environment. The previously reported presence of mitochondria in the terminals suggests a special energy requirement associated with the ionic and molecular exchange and homeostasis (Colombo, 2018). However, the functions of the terminal bulbs require further study.

In addition to the horizontal laminae, neurons in the cerebral cortex are organized vertically into columns, which are parallel to the interlaminar processes (Mountcastle, 1997). It is not known whether the organized structure of neuronal columns serves as the prerequisite for the development of interlaminar processes. Reciprocally, interlaminar astrocytes have been shown to come in close contact with MAP2 positive dendrites (Falcone et al., 2019) and here we show interaction with VGLUT1 positive presynaptic terminals, but whether interlaminar astrocyte activity modulates neuronal activity is yet to be investigated. Changes in cytosolic calcium are considered a major form of astrocytic signaling (Bazargani & Attwell, 2016) but the calcium signaling properties of interlaminar astrocytes have not been studied so far. It is possible that the propagation of calcium waves along the long processes of the interlaminar astrocytes could contribute to rapid communication over long distances thereby modulating neuronal activity across multiple layers. Transduction of hiPSC-astrocytes with genetically encoded calcium indicators before engraftment would allow to determine the spatiotemporal calcium signaling properties of these astrocytes. Moreover, this mouse model provides an opportunity to perform in vivo multilayer recordings of neuronal activity to determine whether and how interlaminar astrocyte processes, that span multiple laminae, impact neuronal activity across the neuronal columns.

Finally, the structural properties of interlaminar astrocytes were found to be altered in some neurological diseases. In brain samples of Down Syndrome patients, a high proportion of the cortex showed disrupted interlaminar processes (Colombo et al., 2005). In addition, in some cases of Alzheimer's disease, interlaminar processes disappeared and instead reactive astrocytes were observed (Buldyrev et al., 2000; Colombo, Quinn, & Puissant, 2002). The use of patient-derived hiPSC-astrocytes and the chimeric mouse model provides an opportunity to study how interlaminar astrocyte structure and functions are altered in other neurodevelopmental and neurodegenerative diseases, enabling researchers to identify novel and astrocyte-related therapeutic strategies.

AUTHOR CONTRIBUTIONS

Baiyan Ren and Yoosun Jung differentiated the cells. Ragunathan Padmashri engrafted the cells. Ryan Gough and Braden Oldham performed immunostaining and Ragunathan Padmashri and Braden Oldham performed confocal imaging. Baiyan Ren performed image analysis. Anna Dunaevsky, Baiyan Ren, and Ragunathan Padmashri wrote the manuscript. Anna Dunaevsky supervised the project and acquired funding.

PEER REVIEW

The peer review history for this article is available at https://publons.com/publon/10.1002/cne.24979.

DATA AVAILABILITY STATEMENT

The data in support of this study are available from the corresponding author upon reasonable request.

ORCID

Anna Dunaevsky [ID] https://orcid.org/0000-0002-0172-9448

REFERENCES

Araque, A., Li, N., Doyle, R. T., & Haydon, P. G. (2000). SNARE protein-dependent glutamate release from astrocytes. *The Journal of Neuroscience*, *202*, 666–673.

Baldwin, K. T., & Eroglu, C. (2017). Molecular mechanisms of astrocyte-induced synaptogenesis. *Current Opinion in Neurobiology*, *45*, 113–120.

Bayer, S. A., & Altman, J. (1991). *Neocortical development*. New York, NY: Raven Press.

Bazargani, N., & Attwell, D. (2016). Astrocyte calcium signaling: The third wave. *Nature Neuroscience*, *192*, 182–189.

Buldyrev, S. V., Cruz, L., Gomez-Isla, T., Gomez-Tortosa, E., Havlin, S., Le, R., … Hyman, B. T. (2000). Description of microcolumnar ensembles in association cortex and their disruption in Alzheimer and Lewy body dementias. *Proceedings of the National Academy of Sciences of the United States of America*, *9710*, 5039–5043.

Canals, I., Ginisty, A., Quist, E., Timmerman, R., Fritze, J., Miskinyte, G., … Ahlenius, H. (2018). Rapid and efficient induction of functional astrocytes from human pluripotent stem cells. *Nature Methods*, *159*, 693–696.

Chen, C., Jiang, P., Xue, H., Peterson, S. E., Tran, H. T., McCann, A. E., … Deng, W. (2014). Role of astroglia in Down's syndrome revealed by patient-derived human-induced pluripotent stem cells. *Nature Communications*, *5*, 4430.

Coiro, P., Padmashri, R., Suresh, A., Spartz, E., Pendyala, G., Chou, S., … Dunaevsky, A. (2015). Impaired synaptic development in a maternal immune activation mouse model of neurodevelopmental disorders. *Brain, Behavior, and Immunity*, *50*, 249–258.

Colombo, J. (2018). Interlaminar glia and other glial themes revisited: Pending answers following three decades of glial research. *Neuroglia*, *11*, 7–20.

Colombo, J. A., Gayol, S., Yanez, A., & Marco, P. (1997). Immunocytochemical and electron microscope observations on astroglial interlaminar processes in the primate neocortex. *Journal of Neuroscience Research*, *484*, 352–357.

Colombo, J. A., Lipina, S., Yanez, A., & Puissant, V. (1997). Postnatal development of interlaminar astroglial processes in the cerebral cortex of primates. *International Journal of Developmental Neuroscience*, *157*, 823–833.

Colombo, J. A., Quinn, B., & Puissant, V. (2002). Disruption of astroglial interlaminar processes in Alzheimer's disease. *Brain Research Bulletin*, *582*, 235–242.

Colombo, J. A., & Reisin, H. D. (2004). Interlaminar astroglia of the cerebral cortex: A marker of the primate brain. *Brain Research*, *10061*, 126–131.

Colombo, J. A., Reisin, H. D., Jones, M., & Bentham, C. (2005). Development of interlaminar astroglial processes in the cerebral cortex of control and Down's syndrome human cases. *Experimental Neurology*, *1931*, 207–217.

Falcone, C., Wolf-Ochoa, M., Amina, S., Hong, T., Vakilzadeh, G., Hopkins, W. D., … Martinez-Cerdeno, V. (2019). Cortical interlaminar astrocytes across the therian mammal radiation. *The Journal of Comparative Neurology*, *52710*, 1654–1674.

Forscher, P., & Smith, S. J. (1988). Actions of cytochalasins on the organization of Actin filaments and microtubules in a neuronal growth cone. *The Journal of Cell Biology*, *107*, 1505–1516.

Han, X., Chen, M., Wang, F., Windrem, M., Wang, S., Shanz, S., … Nedergaard, M. (2013). Forebrain engraftment by human glial progenitor cells enhances synaptic plasticity and learning in adult mice. *Cell Stem Cell*, *123*, 342–353.

Hirabayashi, Y., & Gotoh, Y. (2005). Stage-dependent fate determination of neural precursor cells in mouse forebrain. *Neuroscience Research*, *514*, 331–336.

Hodge, R. D., Bakken, T. E., Miller, J. A., Smith, K. A., Barkan, E. R., Graybuck, L. T., … Lein, E. S. (2019). Conserved cell types with divergent features in human versus mouse cortex. *Nature*, *5737772*, 61–68.

Jones, V. C., Atkinson-Dell, R., Verkhratsky, A., & Mohamet, L. (2017). Aberrant iPSC-derived human astrocytes in Alzheimer's disease. *Cell Death & Disease*, *83*, e2696.

Khakh, B. S., & Deneen, B. (2019). The emerging nature of astrocyte diversity. *Annual Review of Neuroscience*, *42*, 187–207.

Khakh, B. S., & Sofroniew, M. V. (2015). Diversity of astrocyte functions and phenotypes in neural circuits. *Nature Neuroscience*, *187*, 942–952.

Krencik, R., van Asperen, J. V., & Ullian, E. M. (2017). Human astrocytes are distinct contributors to the complexity of synaptic function. *Brain Research Bulletin*, *129*, 66–73.

Miller, F. D., & Gauthier, A. S. (2007). Timing is everything: Making neurons versus glia in the developing cortex. *Neuron*, *543*, 357–369.

Mountcastle, V. B. (1997). The columnar organization of the neocortex. *Brain*, *120* (Pt 4, 701–722.

Oberheim, N. A., Goldman, S. A., & Nedergaard, M. (2012). Heterogeneity of astrocytic form and function. *Methods in Molecular Biology*, *814*, 23–45.

Oberheim, N. A., Takano, T., Han, X., He, W., Lin, J. H., Wang, F., … Nedergaard, M. (2009). Uniquely hominid features of adult human astrocytes. *The Journal of Neuroscience*, *2910*, 3276–3287.

Oberheim, N. A., Wang, X., Goldman, S., & Nedergaard, M. (2006). Astrocytic complexity distinguishes the human brain. *Trends in Neurosciences*, *2910*, 547–553.

Oksanen, M., Petersen, A. J., Naumenko, N., Puttonen, K., Lehtonen, S., Gubert Olive, M., … Koistinaho, J. (2017). PSEN1 mutant iPSC-derived model reveals severe astrocyte pathology in Alzheimer's disease. *Stem Cell Reports*, *9*, 1885–1897.

Olsen, M. L., Khakh, B. S., Skatchkov, S. N., Zhou, M., Lee, C. J., & Rouach, N. (2015). New insights on astrocyte ion channels: Critical for homeostasis and neuron-glia signaling. *The Journal of Neuroscience*, *3541*, 13827–13835.

Reisin, H. D., & Colombo, J. A. (2004). Glial changes in primate cerebral cortex following long-term sensory deprivation. *Brain Research*, *10001-2*, 179–182.

Russo, F. B., Freitas, B. C., Pignatari, G. C., Fernandes, I. R., Sebat, J., Muotri, A. R., & Beltrao-Braga, P. C. B. (2017). Modeling the interplay between neurons and astrocytes in autism using human induced pluripotent stem cells. *Biological Psychiatry*. *83*(7), 569–578. doi:10.1016/j.biopsych.2017.09.021

Sofroniew, M. V., & Vinters, H. V. (2010). Astrocytes: Biology and pathology. *Acta Neuropathologica*, *1191*, 7–35.

Taupin, P., & Gage, F. H. (2002). Adult neurogenesis and neural stem cells of the central nervous system in mammals. *Journal of Neuroscience Research*, *696*, 745–749.

Vainchtein, I. D., Chin, G., Cho, F. S., Kelley, K. W., Miller, J. G., Chien, E. C., … Molofsky, A. V. (2018). Astrocyte-derived interleukin-33 promotes microglial synapse engulfment and neural circuit development. *Science*, *359*, 1269–1273.

Van Horn, M. R., & Ruthazer, E. S. (2018). Glial regulation of synapse maturation and stabilization in the developing nervous system. *Current Opinion in Neurobiology*, *54*, 113–119.

Verkhratsky, A., & Nedergaard, M. (2018). Physiology of Astroglia. *Physiological Reviews*, *981*, 239–389.

Windrem, M. S., Osipovitch, M., Liu, Z., Bates, J., Chandler-Militello, D., Zou, L., … Goldman, S. A. (2017). Human iPSC glial mouse chimeras reveal glial Contributions to schizophrenia. *Cell Stem Cell*, *21*, 195–208.e6.

Zhang, Y., Sloan, S. A., Clarke, L. E., Caneda, C., Plaza, C. A., Blumenthal, P. D., … Barres, B. A. (2016). Purification and characterization of progenitor and mature human astrocytes reveals transcriptional and functional differences with mouse. *Neuron*, *891*, 37–53.

SUPPORTING INFORMATION

Additional supporting information may be found online in the Supporting Information section at the end of this article.